

Reduced thermal conductivity in molecular forests

Aashish Bhardwaj,¹ A. Srikantha Phani,¹ Alireza Nojeh,^{2,3} and Debashish Mukherji^{3,*}

¹Department of Mechanical Engineering, University of British Columbia, Vancouver BC V6T 1Z4, Canada

²Department of Electrical and Computer Engineering,
University of British Columbia, Vancouver BC V6T 1Z4, Canada

³Quantum Matter Institute, University of British Columbia, Vancouver BC V6T 1Z4, Canada

Heat propagation in quasi-one dimensional materials (Q1DMs) often appears paradoxical. While an isolated Q1DM, such as a nanowire, carbon nanotube, or polymer, can exhibit a high thermal conductivity κ , forests of the same materials show a reduction in κ . Here, the complex structures of these assemblies have hindered the emergence of a clear molecular picture of this intriguing phenomenon. We combine multiscale (coarse-grained) simulation with the concepts known from polymer physics and thermal transport to unveil a generic (microscopic) picture of κ reduction in molecular forests. We show that a delicate balance between the bond orientations, the persistence length of the Q1DM and the flexural vibrations govern the knock-down of κ .

Thermal transport properties are important for heat management in devices, energy generation and storage, electronic packaging, house-hold items, bio-materials and interfacial composites, to name a few examples [1–6]. A low thermal conductivity κ is extremely desirable for thermoelectrics [7–9], while very high κ values are needed for heat sinking applications [3, 10, 11]. The ability to tune thermal properties is thus broadly important, and nanoscale systems present a great opportunity in this regard, because they often lead to unique and unexpected behavior [12, 13].

Understanding heat transport in quasi-one dimensional materials (Q1DMs) is a scientifically major problem [12, 13], and becomes even more challenging when dealing with arrays of Q1DMs, such as forests [14–18], bundles [19], sheets [20], and fibers [21, 22]. Here, the complex molecular structure of an array introduces entropic disorder and thus controls its physical properties. One such intriguing phenomenon is strong heat localization in carbon nanotube (CNT) forests [14]: while a single CNT exhibits $\kappa_{||} > 10^3 \text{ Wm}^{-1}\text{K}^{-1}$ [2, 4, 5], CNT forests show a drastic reduction in $\kappa_{||}$. Here, $\kappa_{||}$ is the thermal conductivity along the molecular backbone. This “heat trap” effect was observed at a very high temperatures of $T > 10^3 \text{ K}$. However, room temperature experiments have also yielded relatively low values, such as $\kappa_{||} \simeq 0.5 - 1.2 \text{ Wm}^{-1}\text{K}^{-1}$ for CNT forests [18], $\kappa_{||} \simeq 100 \text{ Wm}^{-1}\text{K}^{-1}$ for CNT bundles [19] or $\kappa_{||} \simeq 43 \text{ Wm}^{-1}\text{K}^{-1}$ for CNT sheets [20]. We note that the observed influence of crowding on $\kappa_{||}$ in CNT forests and sheets may not be a system specific phenomenon. Other examples include nanowire (NW) arrays [15–17], polyethylene (PE) fibers [21], crystalline-like assemblies of PE [22] and poly-3,4-ethylenedioxythiophene (PEDOT) [23], and composite materials [24].

Heat transport in an isolated Q1DM has been studied extensively [12, 13, 25–29]. A few studies have also investigated the effects of crowding on κ , where individual molecules are randomly orientated in a sample [30, 31]. In these studies, the non-bonded van der Waals

(vdW) contacts between different Q1DMs strongly influence their thermal behavior, especially when the molecular lengths are smaller than the sample dimensions. This vdW-based interaction also leads to a low κ [30]. A molecular forest, however, is inherently anisotropic, and a delicate balance between the bonded interactions and molecular entanglements dictates the behavior of $\kappa_{||}$ along the molecular orientations. In the lateral directions, κ_{\perp} is dominated by the weak vdW interaction. Generally, κ between pure bonded neighbors is about 50–100 times larger than that between the non-bonded neighbors [21]. Therefore, it is rather challenging to predict *a priori* how crowding can account for a large drop in $\kappa_{||}$ [14, 16, 17, 20, 22, 23].

In this work we study the anisotropic heat flow in molecular forests using a multiscale molecular simulation approach. For this purpose we: (1) devise a generic scheme to map the nanoscale physics onto a coarse-grained (CG) model, (2) develop a microscopic understanding of the reduced heat transport in molecular forests, and (3) show how a broad range of materials can be modelled within one unified physical concept. To achieve the above goals, we combine molecular dynamics simulations of a generic polymer brush model with known theoretical concepts from polymer physics [32] and thermal transport [33, 34].

We consider a Q1DM as a linear polymer chain, where the inherent flexibility is dictated by its persistence length ℓ_p . For example, a linear molecule behaves as a rigid rod when the contour length $\ell_c \simeq \ell_p$, while it follows a self-avoiding random walk statistics for $\ell_c \gg \ell_p$ [32]. A recent experiment estimated that ℓ_p of an isolated single wall CNT is about 50 – 60 μm for a CNT diameter of $\mathcal{D} \simeq 1.0 \text{ nm}$ [35]. Furthermore, $\ell_p \simeq 5 \mu\text{m}$ for a NW with $\mathcal{D} \simeq 1.0 \text{ nm}$ [36], $\ell_p \simeq 0.65 \text{ nm}$ for PE [37] and $\ell_p \simeq 0.5 - 1.5 \text{ nm}$ for PEDOT [38]. Using these ℓ_p values, we can now analyze molecular forests. For example, the typical heights \mathcal{H} of CNT forests or arrays of NWs range within 0.1 – 2 mm [14, 39] and in some cases can also be 6 mm [18]. For the bundles of PE [21] or PEDOT [23],

$\mathcal{H} \simeq 100$ nm. Therefore, it is evident that $\mathcal{H} \simeq 2 - 200\ell_p$ in most cases. This observation provides an important length scale in our simulations and suggests that a long Q1DM can be modelled as a flexible polymer chain, and hence a molecular forest as a polymer brush. Furthermore, the (covalently) bonded monomers along a chain backbone impart almost crystalline-like structure, while the vdW interactions dominating in the lateral directions induce an amorphous-like two-dimensional packing. This is very similar to the situation in molecular forests [14, 16, 17, 20, 22, 23]. It should be emphasized that, while a simple polymer model is certainly not appropriate to describe all the complex properties of Q1DMs, our aim is to investigate if a CG model can explain the anomalies in thermal behavior observed in experiments [14, 19, 20].

For this study, we employ the bead-spring polymer model [40]. In this model, individual monomers interact with each other via a repulsive 6–12 Lennard-Jones potential with a cutoff distance $r_c = 2^{1/6}d$. $V_{LJ} = 0$ for $r > r_c$. The bonded monomers in a chain interact with an additional finitely extensible nonlinear elastic (FENE) potential. The results are presented in the unit of LJ energy ε , LJ distance d and mass m of individual monomers. This leads to a time unit of $\tau = d(m/\varepsilon)^{1/2}$. We consider chains of length $N_\ell = 500$. Note that ℓ_p of the fully flexible polymer model is about one bead, thus in our case $N_\ell \simeq 500\ell_p$. Here the bond length $\ell_b \simeq 0.97d$. Furthermore, the first monomer of every chain is tethered randomly onto a square plane with lateral dimensions $L_x = L_y \simeq 36.5d$ and the chains are oriented normal to the surface, in the z direction. The surface coverage Γ is varied up to 0.65. Periodic boundary conditions are applied in the x and y directions. One set of single chain simulations have also been performed where the chain is tethered at both ends forming a fully stretched configuration. Further simulation details are shown in the Supplementary Section S1 and Fig. S1 [41].

Simulations are carried out in two stages: the initial equilibration and the thermal transport calculations. Initial equilibration is performed under the canonical ensemble with a time step of $\Delta t = 0.01\tau$ for 2×10^7 MD time steps. The equations of motion are integrated using the velocity Verlet algorithm [42]. The system is thermalized via a Langevin thermostat with a damping constant $\gamma = 1\tau^{-1}$ and $T = 1\varepsilon/k_B$, where k_B is the Boltzmann constant. After this step, the components of κ are calculated using the Kubo-Green method in microcanonical ensemble [43]. More details on κ calculations are in the Supplementary Section S2 and Fig. S2 [41].

In Fig. 1 we summarize the normalized thermal conductivity along a chain backbone $\bar{\kappa}_{||} = \kappa_{||}(\Gamma)/\kappa_{||}(0)$ as a function of Γ . Here, $\kappa_{||}(0)$ corresponds to the single chain data (i.e., $\Gamma \rightarrow 0$). Note that for the calculation of $\kappa_{||}$ in a brush we only consider one chain in the crowded environment. It can be seen that, within the range $0.05 < \Gamma < 0.30$, $\kappa_{||}$ reduces by a factor of 25–30

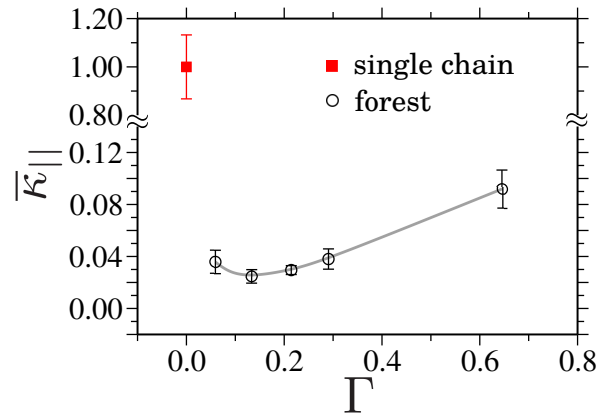


FIG. 1: Normalized thermal conductivity along a chain backbone $\bar{\kappa}_{||} = \kappa_{||}(\Gamma)/\kappa_{||}(0)$ as a function of surface coverage of polymers Γ . $\kappa_{||}(0)$ corresponds to the single chain data (i.e., $\Gamma \rightarrow 0$), where the chain is tethered at both ends. For the simulations under crowded environments, we have only calculated $\kappa_{||}$ of a single chain in a brush configuration, such that a chain experiences a cylinder-like confinement. Note that normalization volume in the Kubo-Green formula is taken as the volume of one chain, i.e., $v = v_m N_\ell$ with v_m being the volume of one monomer. The gray line is a polynomial fit to the data that is drawn to guide the eye.

in a brush compared to a single chain. This sharp decrease is reminiscent of the reduced $\kappa_{||}$ in CNT forests [14, 19] and sheets [20]. What causes such a dramatic decrease in $\kappa_{||}$? It is particularly puzzling given that $\Gamma \gg \Gamma^*$ in all cases (see the Supplementary Table S1 [41]) and therefore individual chains in a brush are expected to stretch significantly [32]. Here, $\kappa_{||}$ is expected to be dominated by the bonded interactions. In this context, a closer investigation reveals that a monomer of a chain in a crowded environment has two different modes of heat dissipation: (a) two covalently bonded neighbors and (b) n non-bonded neighbors governed by the vdW interactions. Furthermore, the vdW interaction strength is less than $k_B T$, while the bonded interactions can be typically of the order of $80k_B T$ (a number representative of a C-C covalent bond) [44, 45]. The stronger bonded interaction also leads to about two orders of magnitude higher stiffness [46, 47]. Moreover, given that κ is directly related to the stiffness (we will come back to this point later) [33, 34], we will now investigate how a 25–30 times reduction in $\kappa_{||}$ is observed in Fig. 1 and in experiments [14, 18–20]. For this purpose, we will now investigate the influence of microscopic chain conformation on $\kappa_{||}$.

We start by calculating the second Legendre polynomial P_2 of the bond orientation vector using $P_2 = (3 \langle \cos^2(\theta) \rangle - 1) / 2$. Here, θ is the angle of a bond vector with the z axis and $\langle \cdot \rangle$ represents the averages over all bonds and the simulation time. Here, $P_2 = 1.0$ when all bonds are oriented along the z axis, $P_2 = 0.0$ when bonds are randomly oriented and $P_2 = -1/2$ when all

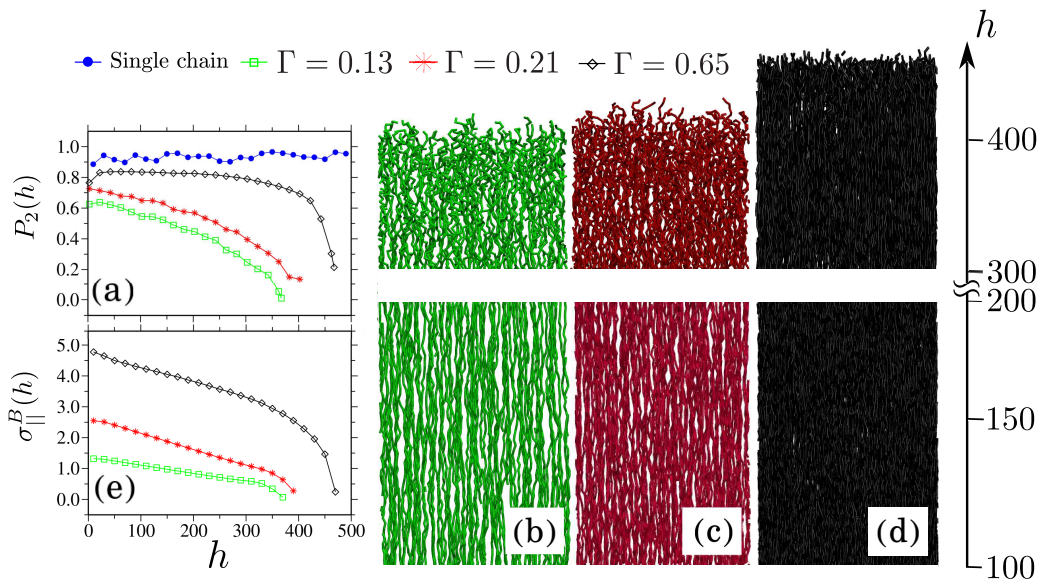


FIG. 2: (a) shows the second Legendre polynomial of the bond orientation vector P_2 as a function of the brush height h along the z axis. Data is shown for a single chain and for three different surface coverage concentration Γ . (b-d) show simulation snapshots for $\Gamma = 0.13$ (green), $\Gamma = 0.21$ (red) and $\Gamma = 0.65$ (black). The bottom panels of the snapshots are the enlarged views of brushes between $100d < h < 200d$ and the top panels show the top layer for $h > 340d$. The arrow at the right corner points at the direction of brush height h . (e) is the same as (a) but for the stress along the chain backbone $\sigma_{||}^B$. The lines are drawn to guide the eye.

bonds are perpendicular to the z axis. In Fig. 2(a) we show the variation of P_2 with the forest height h for three different values of Γ . It can be seen that $P_2 \simeq 0.92$ for a single polymer with about 5% fluctuation. This is expected given that a single chain is fully stretched and all bonded monomers are arranged in an almost perfect one-dimensional crystalline-like structure along the z axis. This is also consistent with a large $\kappa_{||}$ value for a single chain (see Fig. 1).

For $\Gamma = 0.13$ and $\Gamma = 0.21$ in Fig. 2(a), it can be seen that P_2 decreases rather sharply with h , as known from the structure of polymer brushes [48]. This is consistent with the tethering constraint that the chains are significantly more stretched near the tethered points and become more randomly oriented as h increases, see also simulation snapshots in Figs. 2(b-c). Furthermore, the individual chain end-to-end distances are $R_{ee}^z \simeq 370d$ (for $\Gamma = 0.13$) and $R_{ee}^z \simeq 380d$ (for $\Gamma = 0.21$) (see the Supplementary Table S1 and Fig. S1 [41]), and thus are only about 75% of the chain contour length $\ell_c = N_\ell \ell_b \simeq 485d$ for $N_\ell = 500$. This incompatibility between R_{ee}^z and ℓ_c indicates a significant chain bending (via the flexural vibrations) and thus introduces a large degree of intra-chain entanglements, also visible from the lower panels of the simulation snapshots in Figs. 2(b-c). With increasing h , chain bending and entanglement become more-and-more prominent, see the upper panels of the simulation snapshots in Figs. 2(b-c). In this context, it is important to note that in a fully stretched chain (as in our case of the single chain), phonon-like wave propagation car-

ries a heat current along the chain backbone because of the periodic arrangement of monomers. When entanglements appear along a chain backbone due to the flexural vibrations dictated by ℓ_p (as in the cases of $\Gamma = 0.13$ and 0.21), the longitudinal phonon propagation is impacted. Here, each entanglement acts as a scattering center for phonon propagation and thus reduces the phonon mean free path. The larger the number of entanglements for a given N_ℓ , the higher the resistance to heat flow, i.e., the lower $\kappa_{||}$ (see Fig. 1). This observation is consistent with the recent simulation study of a single PE chain, where it has been shown that increasing the number of kinks also decreases κ [49]. For $\Gamma = 0.65$, bonds are significantly more oriented and also the chains are more stretched with $R_{ee}^z \simeq 450d$ (see Figs. 2(a) and (d)), resulting in an approximately three fold increase of $\kappa_{||}$ in comparison to $\Gamma = 0.13$ or 0.21 , see Fig. 1

Chain bending also reduces the longitudinal chain stiffness and thus κ . Therefore, to achieve a better quantitative relationship between P_2 (or an estimate of bending), local stiffness, and κ , we will now look into how P_2 can be related to stiffness (or stress). For this purpose, we have calculated the h dependent bonded contribution to the virial stress $\sigma_{||}^B$. The data is shown in Fig. 2(e). It can be seen that the data for $\Gamma = 0.13$ and 0.21 not only show a rather large variation with h , consistent with the variation of P_2 in Fig. 2(a), but that this is significantly lower than $\sigma_{||}^B \simeq 5.0 \epsilon d^{-3}$ for $\Gamma = 0.65$, see Fig. 2(e).

Figs. 2(a) and (e) also suggest that there is an inherent h dependent anisotropy in the chain orientation, i.e., the

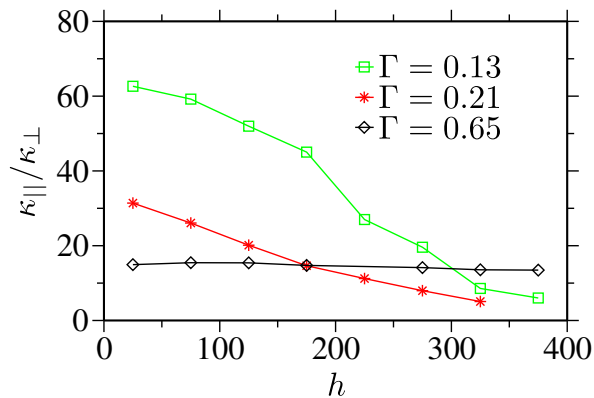


FIG. 3: $\kappa_{||}/\kappa_{\perp}$ as a function of the brush height h . Here, $\kappa_{||}$ and κ_{\perp} are the parallel and the perpendicular components of the thermal conductivity, respectively. Data are shown for three different surface coverage concentrations Γ . The lines are drawn to guide the eye.

chains are more stretched very close to $h \rightarrow 0$ due to tethering and become more random with increasing h [32, 48]. Consequent anisotropy is reflected in $\kappa_{||}/\kappa_{\perp}$ in Fig. 3, where κ_{\perp} is the thermal conductivity along the x & y directions. For $\Gamma = 0.13$ we observe that heat flow is: highly anisotropic for $h < 200d$ ($\kappa_{||}/\kappa_{\perp} \simeq 50 - 60$), moderately anisotropic for $200d < h < 350d$ ($\kappa_{||}/\kappa_{\perp} \simeq 10 - 40$), and weakly anisotropic for $h > 350d$ ($\kappa_{||}/\kappa_{\perp} < 10$). With increasing Γ , the relative anisotropy in $\kappa_{||}/\kappa_{\perp}$ decreases (see the red and black data sets in Fig. 3). This is predominantly because of the increased particle number density ρ that induces a faster increase in κ_{\perp} than $\kappa_{||}$ with ρ (see the Supplementary Figs. S1 & S3 and Section S2 [41]). Here, considering that $\ell_p \simeq 1d$ in our model, this also gives a comparable estimate of the relevant length scales (in terms of ℓ_p) that are needed to make a direct experimental comparison. In this context, most experiments on CNT forests deal with $\Gamma \leq 0.10$, $1 < \mathcal{D} < 10$ nm (can even be several 10 nm in some cases) and also relatively small $\mathcal{H} \leq 2$ mm [14]. Therefore, the conditions typically fall within the range when \mathcal{H} varies from a few ℓ_p to about $40\ell_p$ (i.e., for $\mathcal{D} \simeq 1.0$ nm and $\mathcal{H} \simeq 2$ mm) [35]. This will then lead to a rather anisotropic regime [14, 20]. Here, experiments on CNT forests yielded a $\kappa_{||}/\kappa_{\perp} \simeq 10 - 100$ [14, 18], for CNT sheets $\kappa_{||}/\kappa_{\perp} \simeq 500$ [20], and for PE fibers $\kappa_{||}/\kappa_{\perp} \simeq 1000$ [21]. Furthermore, our simulations show $\kappa_{||}/\kappa_{\perp} \simeq 10 - 60$ for $h < 200\ell_p$ and with varying Γ , see Fig. 3. This further suggests that our simple CG model captures the relevant physics of the problem.

Lastly, Fig. 4 shows $\kappa_{||}$ as a function of an estimate of elastic modulus along the direction of the chain orientation $\sigma_{||}^B/\mathcal{E}$. Here, \mathcal{E} is strain. We estimate \mathcal{E} from the stretching of the bond vector along the z direction. It can be appreciated that the data in Fig. 4 is constant with an understanding that κ is directly related to the

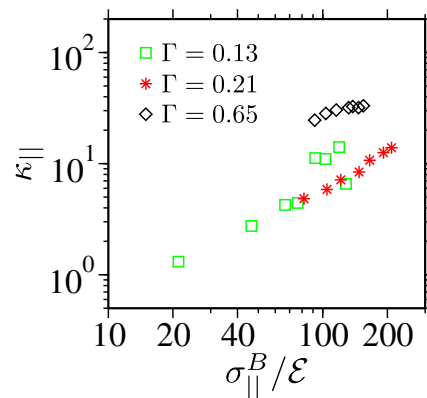


FIG. 4: The parallel component of the thermal conductivity $\kappa_{||}$ as a function of an estimated elastic modulus along the chain orientation $\sigma_{||}^B/\mathcal{E}$. Here, $\sigma_{||}^B$ and \mathcal{E} are the longitudinal bonded components of the stress and strain, respectively. Data are shown for three different surface coverage concentrations Γ .

stiffness [33, 34].

In conclusion, combining molecular dynamics simulations with known concepts from polymer physics and thermal conductivity, we have studied the microscopic, generic behavior of anisotropic thermal conductivity in molecular forests. As a model system, we have used a generic coarse-grained polymer brush. We provide a possible explanation for the reduced thermal conductivity in molecular forests, i.e., the observation that, while a single linear molecule can have very large thermal conductivity along the molecular backbone $\kappa_{||}$, the same molecule in a forest shows a drastic reduction in $\kappa_{||}$. Typical experimental systems include nanotube and nanowire forests and macromolecular fibers. Our analysis reveals that the reduced $\kappa_{||}$ is due to the lateral chain bending that hinders the longitudinal heat flow along the molecular backbone. These results point to a general principle of flexible tuning of κ by changing density, molecular flexibility and forest height. Therefore, they may pave the way towards the design of advanced functional materials with tunable thermal properties.

We thank George Sawatzky, Daniel Bruns and Manjesh Singh for useful discussions. We further thank Celine Ruscher for a critical reading of the manuscript. This research was undertaken thanks in part to funding from the Canada First Research Excellence Fund, Quantum Materials and Future Technologies Program. S.P. thanks NSERC Discovery Grant program for support. A.N. acknowledges financial support from the Natural Sciences and Engineering Research Council of Canada (Grants No. SPG-P 478867, jointly with S.P., and No. RGPIN-2017-04608). D.M. thanks the Canada First Research Excellence Fund (CFREF) for the financial support. Simulations were performed at the ARC Sockeye facility of the University of British Columbia and

the Compute Canada facility, which we take this opportunity to gratefully acknowledge. Simulations in this manuscript were performed using the LAMMPS molecular dynamics package [50] and the simulation snapshots were rendered using the VMD package [51].

* debashish.mukherji@ubc.ca

- [1] D. G. Cahill, W. K. Ford, K. E. Goodson, G. D. Mahan, A. Majumdar, H. J. Maris, R. Merlin, and S. R. Phillpot, *J Appl. Phys.* **93**, 793 (2003).
- [2] S. Berber, Y.-K. Kwon, and D. Tomanek, *Phys. Rev. Lett.* **84**, 4613 (2000).
- [3] G. Kim, D. Lee, A. Shanker, L. Shao, M. S. Kwon, D. Gidley, J. Kim, and K. P. Pipe, *Nat. Mat.* **14**, 295 (2015).
- [4] V. Lee, C.-H. Wu, Z.-X. Lou, W.-L. Lee, and C.-W. Chang *Phys. Rev. Lett.* **118**, 135901 (2017).
- [5] Q.-Y. L, K. Takahashi, and X. Zhang, *Phys. Rev. Lett.* **119**, 179601 (2017).
- [6] G. Fugallo and L. Colombo, *Phys. Scri.* **93**, 043002 (2018).
- [7] D. Teweldebrhan, V. Goyal, and A. A. Balandin, *Nano lett.* **10**, 1209 (2010).
- [8] T. Kodama, M. Ohnishi, W. Park, T. Shiga, J. Park, T. Shimada, H. Shinohara, J. Shiomi and K. E. Goodson, *Nat. Mat.* **16**, 892 (2017).
- [9] W. Shi, Z. Shuai and D. Wang, *Adv. Funct. Mater.* **27**, 702847 (2017).
- [10] S. Ren, M. Bernardi, R. R. Lunt, V. Bulovic, J. C. Grossman, and S. Gradecak, *Nano lett.* **11**, 5316 (2011).
- [11] M. K. Smith, V. Singh, K. Kalaitzidou, and B. A. Cola, *ACS Appl. Mater. Int.* **8**, 14788 (2016).
- [12] A. M. Marconnet, M. A. Panzer and K. E. Goodson, *Rev. Mod. Phys.* **85**, 1295 (2003).
- [13] J. C. Charlier, X. Blase and S. Roche, *Rev. Mod. Phys.* **79**(2) , 677 (2007).
- [14] P. Yaghoobi, M. V. Moghaddam and A. Nojeh, *Sol. Stat. Comm.* **151**, 1105 (2011).
- [15] J. P. Feser, J. S. Sadhu, B. P. Azeredo, K. H. Hsu, J. Ma, J. Kim, M. Seong, N. X. Fang, X. Li, P. M. Ferreira, S. Sinha, and D. G. Cahill, *J. App. Phys* **112**, 114306 (2012).
- [16] Y. Pan, G. Hong, S. N. Raja, S. Zimmermann, M. K. Tiwari, and D. Poulikakos, *App. Phys. Lett.* **106**, 093102 (2015).
- [17] G. Pennelli, S. Elyamny and E. Dimaggio., *Nanotechnology* **29**, 505402 (2018).
- [18] M. B. Jakubinek, M. A. White, G. Li, C. Jayasinghe, W. Cho, M. J. Schulz, and V. Shanov, *Carbon* **48**, 3947 (2010).
- [19] M. B. Jakubinek, *Nanotube Superfiber Materials, Chapter 16: Thermal Conductivity of Nanotube Assemblies and Superfiber Materials* 425-456 (2014).
- [20] S. Yamaguchi, I. Tsunekawa, N. Komatsu, W. Gao, T. Shiga, T. Kodama, J. Kono, and J. Shiomi, *App. Phys. Lett.* **115**, 223104 (2019).
- [21] S. Shen, A. Henry, J. Tong, R. Zheng, and G. Chen, *Nat. Nanotech.* **5**, 251 (2010).
- [22] A. Henry, G. Chen, S. J. Plimpton, and A. Thompson, *Phys. Rev. B* **82**, 144308 (2010).
- [23] A. Crnjar, C. Melis, and L. Colombo, *Phys. Rev. Mater.* **2**, 015603 (2018).
- [24] *J App. Mech.* **50**, 481 (1983).
- [25] D. Donadio and G. Galli, *Phys. Rev. Lett.* **99**, 255502 (2007).
- [26] A. Henry and G. Chen, *Phys. Rev. Lett.* **101**, 235502 (2008).
- [27] M. N. Ou, T. J. Yang, S. R. Harutyunyan, Y. Y. Chen, C. D. Chen, and S. J. Lai, *App. Phys. Lett.* **92**, 063101 (2008).
- [28] D. Donadio and G. Galli, *Phys. Rev. Lett.* **102**, 195901 (2009).
- [29] J. Lee, W. Lee, J. Lim, Y. Yu, Q. Kong, J. J. Urban, and P. Yang, *Nano Lett.* **16**, 4133 (2016).
- [30] R.S. Prasher, X. J. Hu, Y. Chalopin, N. Mingo, K. Lofgreen, S. Volz, F. Cleri, and P. Keblinski, *Phys. Rev. Lett.* **102**, 105901 (2009).
- [31] A. N. Volkov and L. V. Zhigilei, *App. Phys. Lett.* **101**, 043113 (2013).
- [32] M. Doi, *Soft Matter Physics* Oxford University Press (2013).
- [33] D. G. Cahill, S. K. Watson, and R. O. Pohl, *Phys. Rev. B* **46**, 6131 (1992).
- [34] J. L. Braun, C. M. Rost, M. Lim, A. Giri, D. H. Olson, G. N. Kotsonis, G. Stan, D. W. Brenner, J.P. Maria, and P. E. Hopkins, *Adv. Mat* **30**, 1805004 (2018).
- [35] N. Fakhri, D. A. Tsyboulski, L. Cagnet, R. Bruce Weisman, and M. Pasquali, *Proc. Nat. Acad. Sci.* **106**, 14219 (2009).
- [36] H. Liu, H.-L.Song, X. Feng, and J. Yang, *Theo. App. Mech. Lett.* **4**, 051009 (2014).
- [37] R. Ramachandran, G. Beaucage, A. S. Kulkarni, D. McFaddin J. Merrick-Mack, and V. Galiatsatos, *Macromolecules* **41**, 9802 (2008).
- [38] Editors- J. Brandrup, E. H. Immergut, E. A. Grulke, *Polymer Handbook* (2003).
- [39] N. Yang, M. Li, J. Patscheider, S. K. Youn, and H. G. Park *Sci. Rep.* **7**, 46725 (2017).
- [40] K. Kremer and G. S. Grest, *J Chem. Phys.* **92**, 5057 (1990).
- [41] See supplementary material (Document No. to be filled in by editor).
- [42] W. C. Swope, H. C. Andersen, P. H. Berens, and K. R. Wilson, **76**, 648 (1982).
- [43] R. Zwanzig, *Annu. Rev. Phys. Chem.* **16**, 67 (1965).
- [44] G. P. Desiraju, *Acc. Chem. Res.* **35**, 565 (2002).
- [45] D. Mukherji, C. M. Marques, and K. Kremer, *Ann. Rev. Cond. Mat. Phys.* **11**, 271 (2020).
- [46] B. Crist, and P. G. Herena, *J. Polym. Sci., Part B: Polym. Phys.* **34**, 449 (1996).
- [47] C. Ruscher, J. Rottler, C. E. Boott, M. J. MacLachlan, and D. Mukherji, *Phys. Rev. Mat.* **3**, 125604 (2019).
- [48] K. Binder, *Eur. Phys. J. E* **9**, 293 (2002).
- [49] X. Duan, Z. Li, J. Liu, G. Chen, and X. Li, *J App. Phys.* **125**, 164303 (2019).
- [50] S. Plimpton, *J Comp. Phys.* **117**, 1 (1995).
- [51] W. Humphrey, A. Dalke, and K. Schulten, *J Mol. Graph.* **14**, 33 (1996).